RSC Advances

Journal Name

ARTICLE TYPE

Molecular Insight into the Mode-of-action of Phosphonate Monolayers as Active Functions of Hybrid Metal Oxide Adsorbents. Case study in Sequestration of Rare Earth Elements

Gulaim A. Seisenbaeva,*[a] Inna V. Melnyk,[b] Niklas Hedin,[c] Yang Chen,[d] Philip Eriksson,[a] Elżbieta Trzop,[d] Yuriy L. Zub,[b] and Vadim G. Kessler[b]

The insight into the molecular aspects of ligand grafting and potential maximal capacity of hybrid organic-inorganic adsorbents bearing phosphonate ligand monolayers as active functions was obtained by single crystal X-ray studies of ligand-functionalized titanium alkoxide complexes. The attachment of molecules occurs generally in the tripodal vertical fashion with minimal distance between them being about 8.7 Å, resulting in the 0.19 nm^2 as minimal surface area per function. In the present experimental work almost theoretical loading capacity could be achieved for functionalization of mesoporous nanorods of anatase with imino-bis-methylphosphonic acid (IMPA, $NH(CH_2PO_3H_2)_2$) or aminoethylphosphonic acid (AEPA, $H_2NC_2H_4PO_3H_2$). The products had the same morphology as the starting material, as was established by SEM and optical microscopy. The size and structure of the individual nanoparticles of the constituting inorganic component of the material were preserved and practically unchanged through the surface modification, as established by powder XRD and EXAFS studies. The surface area of the inorganic-organic hybrids decreased somewhat from the initial ~250 m^2/g, on adsorption of AEPA (0.21 mmol/g) – to ~240 m^2/g, and on adsorption of IMPA (0.17 mmol/g) to ~190 m^2/g. The ligands were bound effectively to the surface according to TGA, EDS and FTIR analyses and remained in mono-deprotonated form. The produced hybrid adsorbents had for the selected pH (3.5) high capacities towards adsorption of Rare Earth Element (REE) cations, but with equilibria achieved relatively slowly. The composition of the surface complexes was determined as M:L = 1:1 for IMPA, but varied for the AEPA from 1:3 to 1:1 dependent on the REE, which can be interpreted in the terms of charge compensation as the major driving force behind binding. The cation desorption in strongly acidic media for recuperation of the adsorbed REE and the relative capacity of the re-used adsorbent have been quantified.

Introduction

Highly chemically stable and poorly soluble nanostructured transition metal oxides, in the first hand, TiO_2 and ZrO_2, have already found broad application as adsorbent materials [1, 2]. A large surface charge [3] with a dominating total negative charge in a broad pH interval [4], together with enhanced chemical affinity to highly charged anions makes these materials efficient as adsorbents in immobilization of a broad spectrum of solute species. The adsorbates include heavy metal cations such as uranium and thorium [5], various toxic anions, for example, arsenate $[AsO_4^{3-}]$ [6] and a whole variety of biomolecules carrying carboxylate [7] or, especially, phosphate or phosphonate [8] anchoring moieties forming generally self-assembled monolayers on the oxide surfaces. These features are attractive for extraction and chromatographic separation of in particular DNA and nucleotides,[9] proteins [2, 10] and potentially also phosphorylated carbohydrates. The adsorption processes rely on the molecular details of the interactions on the surfaces, and nanomaterials with their very large surface-to-volume ratio are especially attractive adsorbents. In the case of TiO_2, very large surface-to-volume ratios are available for nanotubes or nanorods produced in high yields by acidification and subsequent exfoliation of layered alkali titanates [11] or simply by electrospinning. [12] Facile and cost-efficient production of porous titania (anatase) nanorods is possible by rapid hydrothermal synthesis. It employs nanorods of a metal-organic precursor titanium methoxide, $Ti(OCH_3)_4$ as starting material. [13] The inexpensive and efficient surfactant-free synthesis of nano titania makes related materials attractive alternatives to mesoporous silica adsorbents and magnetic silicas that have otherwise revealed such attractive characteristics as high adsorption capacity and rapid kinetics.[14]

Titania-based adsorbents can be surface modified for potential uses in various applications using organic monolayers carrying a wide range of organic functionalities. Surface modification

allows TiO_2 nanoparticles to be stabilized in both aqueous [8] and hydrocarbon [15] media. They have also been converted into hybrid organic-inorganic materials with principally changed hydrophilicity/hydrophobicity and functionality, applied, for example, in the sorption of CO_2 from gas mixtures, [16] in separation of hydrophobic dyes from diluted solutions [17] and in extraction of heavy metal cations. [18] Among those a special attention has recently been focused on Rare Earth Elements (REE). REE, and especially neodymium (Nd) and dysprosium (Dy) are required for production of magnetic materials used both in electronics [19] and novel energy production technologies utilizing renewable energy sources, [20] and are available as components in ores abundant in the Northern Europe, Iceland, Greenland, USA and Canada. Their production today is, however, almost exclusively concentrated to China, where they are present in easier exploitable forms and where the environmental hazards associated with their extraction and separation (production of huge volumes of acidic wastes and use of huge volumes of organic solvents) are presently not treated with the same care. Also the adsorption of actinide elements accumulating in the nuclear waste and displaying solution behavior analogous to REE became a topic of increased attention in connection with recent disaster at the Fukushima nuclear plant. [21] An effort has been reported recently in creation of hybrid mesoporous silica based adsorbents bearing alkyl phosphonate function for selective adsorption of REE. [22]

Recently it has been proposed to use mesoporous hybrid organic-inorganic materials based on metal oxides modified by a number of commercially available phosphonic acids as adsorbents for selective extraction of REE, and, in particular, of the radioactive elements originating from nuclear fission such as ^{153}Gd. [23] These studies were carried out at pH = 2 and the adsorbent showed quite modest capacity (0.005 mmol/g).

In the present work the structure of the surface layer and the potential maximal adsorption capacity were elucidated with the help of single crystal X-ray studies of relevant molecular models. The results from studies of hybrid adsorbents produced from mesoporous titania nanorods, derived by a precursor-driven approach [13] via subsequent straightforward immobilization of aminoethylphosphonic acid AEPA ($NH_2(CH_2)_2PO_3H_2$) and imino-bisphosphonic acid IMPA ($NH(CH_2PO_3H_2)_2$) on their surface are discussed.

Experimental

All chemicals and solvents used in this work were obtained from commercial sources and used without further purification. $Ti(OCH_2CH_3)_4$ (99+%) was purchased from Alfa Aesar. Titanium methoxide $Ti(OCH_3)_4$, imino-bis[methylenephosphonic acid], IMPA (CAS number: 17261-34-6), and 2-aminoethyl phosphonic acid, AEPA (CAS number: 2041-14-7), and also, ethanol (200 proof, anhydrous, $\geq$ 99.5%) were purchased from Aldrich. The compounds containing titanium were stored and handled in a standard glove-box under a nitrogen atmosphere. The synthesis of the starting mesoporous anatase was carried out by rapid hydrothermal technique as described earlier. [13]

Synthesis

For surface modification about 1.3 g of the TiO_2 nanorods were dispersed in 26 ml of the aqueous solution of the corresponding phosphonic acid (applied in excess, 2 mmol/g) and kept at room temperature under continuous stirring for 48 h. The product was isolated by sedimentation overnight with subsequent decantation of the solvent and washed by water (3 portions of 26 ml), separated by centrifugation and dried in vacuum during 2h at room temperature. Yield for TiO_2-IMPA was 1.3114 g, TiO_2-AEPA – 1.0421 g.

The synthesis of molecular model compounds was carried out either in acetonitrile/acetone mixed solvent to initiate formation of oxo-species via Bradley reaction, [24] adding 1 eq. of phosphonic acid per 4 eq. of titanium ethoxide or using solvothermal treatment in ethanol medium as described earlier in. [25]

Compound 1, $Ti_4O(EtO)_{12}(^tBuPO_3)$. tert-Butylphosphonic acid (107.8 mg, 0.78 mmol), acetone (265 mg, 4.56 mmol) and acetonitrile (10 mL) were mixed in a round-bottom flask. After stirring the mixture for 1 minute, titanium(IV) ethoxide (1 g, 4.38 mmol) was added to it in a glove box. The mixture was then subjected to reflux for 10minutes and ethanol (5 mL) was added producing again a clear slightly yellowish solution. The flask was sealed and then cooled down and kept at RT for 72 h. Massive precipitation of colorless crystals of **1** was observed.

Compound 2, $Ti_{10}O_2(EtO)_{32}(AEP)_2$, where AEP = 2-aminoethylphoshonate. To a Pyrex glass tube (15 cm in length, 8.14 mm in inner diameter and 11.14 mm in outer diameter) was added titanium(IV) ethoxide (0.10 g, 0.44 mmol), 2-aminoethylphosphonic acid (0.01 g, 0.08 mmol) and ethanol (2.0 mL) in a standard glove-box under a nitrogen atmosphere. The tube was sealed immediately outside the glove-box using a torch, then heated in an oven at 120 °C for 6 days and then slowly cooled to the room temperature in the oven. The mother solution was filtered and left to evaporate in the glove-box. The colorless plate crystals of compound **2** were formed. The crystals of **2** were separated from the solution, washed with ethanol and dried in the glove-box. Yield: 29.5 mg (33.6 % based on 2-Aminoethylphosphonic acid).

Characterization

The analysis for phosphorus was performed by the certified analytical laboratory of Institute of Organic Chemistry of National Academy of Science of Ukraine at the KFK-2 equipment by burning in Shoniger method (Error ±0.3%). The FT-IR spectra were recorded on a Thermo Nicolet Nexus Fourier-transform infrared spectrometer in the 400–4000 cm^{-1} range, working in "Nexus Smart Collector" mode with a resolution of 8 cm^{-1}. The samples were ground with solid KBr («Fluka», for IR-spectroscopy). The sample/KBr mass ratio was 1/30. The imaging was made with JSM-6060LA Analytical Scanning Electron Microscope (Jeol, Tokyo, Japan) using secondary electrons at accelerating voltage of 30 kV. To prevent accumulation of positive charges and to receive good contrast, the surfaces of the samples were covered with thin and continuous layers of gold or platinum by cathodic sputtering under dynamic vacuum conditions. The estimation of the amounts of the adsorbed ligand and metals were carried out by a SEM-EDS technique using a Hitachi TM-1000-µ-DeX tabletop scanning electron microscope (with and estimated error ± 0.20 wt%). X-ray powder patterns were obtained using a Bruker SMART APEX-II diffractometer operating with MoK$_\alpha$ radiation (λ=0.71073 Å). The diffraction

was registered in rotation mode (1 degree/s) for powder samples sealed in 0.7 mm Lindeman tubes. Bruker APEX-II and EVA software were used for integration and data treatment. Thermal characteristics of the prepared powders and the adsorption properties of evacuated samples were studied using a Perkin-Elmer Pyris-1 TGA instrument connected for gas analysis with a Perkin-Elmer Spectrum 100 FTIR instrument (Error ±0.02%). The low temperature nitrogen adsorption-desorption isotherms were recorded with a Kelvin 1042 instrument at –196°C. The samples were pre-degassed at 110°C for 12 h. The specific surface area was calculated by the BET method, [26] and the pore size distribution was determined by the BJH [27] using the desorption branch.

EXAFS data collection. Titanium K edge X-ray absorption spectra were recorded at the wiggler beam line I811 at the MAX-Lab, Lund University, Lund, Sweden. The EXAFS station was equipped with a Si {111} double crystal monochromator. The data collection was performed in luminescence mode. Higher order harmonics were reduced by detuning the second monochromator to 30% of maximum intensity at the end of the scans. The energy scale of the X-ray absorption spectra was calibrated by assigning the first inflection point of the K edge of a titanium foil to 4966 eV. The IFEFFIT program package [28] was used for the data treatment.

[31]P Nuclear Magnetic Resonance (NMR) spectroscopy. Direct polarization solid state ^{31}P NMR spectra were recorded under magic angle spinning at 14 kHz at a frequency of 161.95 MHz on a Bruker Avance III spectrometer. A wide-bore superconductive magnet operating at a field of 9.4 T was used. SPINAL (small phase incremental alteration) decoupling of ^{1}H contributions were applied during acquisition. A recycling delay of 100s was used and 128 scans were acquired for each spectra and an exponential appodization of 50Hz was applied before Fourier transformation. Liquid phase NMR spectra were recorded with a Bruker Avance 600 MHz SMART Probe spectrometer. The ^{31}P NMR chemical shift was externally calibrated with a solution of concentrated H_3PO_4.

pH-potentiometric titration of phosphonic acid groups. Measurement of pH was conducted on 420A Scand Inovatra "Orion". The calibration was performed using standard buffer solutions in accordance with the instructions of the appliance. 0.072 g of sample was poured with 10 cm^3 of 0.1 M NaNO$_3$ solution. NaOH 0.024 M solution was added drop wise and under constant stirring to the resulting mixture. After the equilibrium was established, a change in pH was measured (Error ±1%).

REE adsorption studies. Investigation of Y(III), La(III), Nd(III) and Dy(III) sorption from water solutions of their nitrate salts was carried out in static mode (m = 0.05 g (± 0.0005), V = 20 cm^3, T = 22°C). The ionic strength was maintained by a 0.1mol/dm^3 NaNO$_3$ solution. Concentrations of metals in the initial solutions and after sorption were determined by direct titration of metal ions by EDTA (method error ±1%). [29] In order to achieve an equilibrium the metal ion sorption time was set to 72 h, as established by the quantitative study of the reaction kinetics. The pH conditions of the suspensions were measured after the sorption. The precipitates were washed one time by 10 cm^3 distilled water, and the contents of metals were determined in the filtrate. The difference between the content of metal ions in

solution before and after sorption was used to estimate the adsorption (mmol/g and mmol/l). Desorption (recovery) was carried out in a static mode by adding 5 cm^3 of a 1 mol/dm^3 solution of hydrochloric acid and waiting for 72 h.

Crystallography. The single crystal X-ray diffraction was carried out for compound 1 and 2 respectively at 113 K and 90K using Bruker SMART APEX-II CCD diffractometers equipped with nitrogen flow apparatus. Data integration was carried out using the program SAINT. Absorption corrections were made with the program SADABS. The structures were solved by direct methods and refined by least-squares methods against F^2 using SHELXS-97 and SHELXL-2014.[30] Non-hydrogen atoms were refined anisotropically; all hydrogen atoms were placed in geometrically idealized positions and constrained to ride on their parent atoms. Ti$_4$-oxo core is common for two compounds, 1 and 2. In both cases the Ti$_4$-Oxo core shows significant disorder on one of three titanium atoms sites directly connected with RPO$_3$-ligand where R = tetra-butyl and phenyl group respectively. For compound 1 two alternative positions have been identified around Ti(4) atom site and refined with partial occupancies of 52.2% and 47.8%; for compound 2 two alternative positions have been identify in close proximity to the Ti(1) and Ti(3) atom sites. Refinement gave partial occupancies of 65.5% and 34.5% respectively. In addition most of the ethyl groups attached to the surfaces of **1** and **2** have been treated with a disorder model. Regardless of considerable disorder, charge neutrality of 1 and 2, is preserved. Crystal data and details of the data collection and refinement for **1** and **2** are summarized in Tab. 1. Full details can be found in CCDC-1027996 for **1** and CCDC-1027997 for **2**, which can be obtained free of charge via *www.ccdc.cam.ac.uk/data_request/cif* or at deposit@ccdc.cam.uk (the Cambridge Crystallographic Data Center, 12 Union Road, Cambridge CB2 1EZ, UK; Fax: (+44) 1223-336-033).

Table 1 Crystal data and diffraction experiments' details for compounds **1** and **2.**

Compound	1	2
Chemical composition	$C_{28}H_{69}O_{16}PTi_4$	$C_{68}H_{172}N_2O_{40}P_2Ti_{10}$
Formula weight	884.40	2199.01
Crystal system	Triclinic	Triclinic
Space group	P-1	P-1
Z	2	1
a(Å)	10.7705(12)	11.8405(4)
b(Å)	11.6006(12)	13.7396(5)
c(Å)	20.017(2)	17.3724(6)
α(°)	80.035(4)	77.9838(10)
β(°)	89.067(5)	73.2551(10)
γ(°)	63.258(4)	88.8981(11)
V(Å3)	2194.4(4)	2644.56(16)
T (K)	113(2)	90(2)
Θ range (°)	2.42~24.88	2.29~ 26.71
R1 (I>4σ(I))	0.0635	0.0506
wR2 (I>4σ(I))	0.1673	0.1151
R1 (All data)	0.1011	0.0761
wR2 (All data)	0.1982	0.1324
Goodness-of-fit	1.012	1.051
Number of parameters	735	821
Unique reflections	9504[Rint = 0.0347]	10392[Rint = 0.0414]
Observed reflections (I>4σ(I))	6127	7655

Results and discussion

The aim of this study was to provide molecular insights into grafting of the ligands on the surface of hybrid metal oxide adsorbents and develop and evaluate mesoporous adsorbent
5 materials based on nanorods of TiO_2 with easily available and quite densely grafted adsorption centers.

The structures of molecular model compounds

In the present study we intended to broaden the family of oxo-alkoxotitanate structures modeling the titania nanoparticles [31] and
10 employing both structurally demanding alkyl phosphonate ligands and also the amino alkyl phosphonate ligands to get an insight into the chemical features of grafting these ligands onto metal oxide surface. For realization of this task we chose t-butyl phosphonic acid and aminoethyl phosphonic acid as
15 representatives. Aminoethyl phosphonic acid is poorly soluble in organic solvents and thus an autoclave synthesis was applied. In contrast, t-butyl phosphonic acid has an appreciable solubility even in polar organic solvents and thus we used acetonitrile as medium and acetone as co-solvent to induce formation of oxo-
20 species on short reflux. The latter reaction proceeded with practically quantitative yield. The structure of the obtained derivative **1** (see Fig. 1) turned to be very strongly resembling that of the recently studied phenyl phosphonate analog $Ti_4O(EtO)_{12}(PhenylPO_3)$. [25]
25 The RPO_3-ligand is attached via three $Ti-(\mu-O)-P$ bridges to three titanium atoms Ti(2), Ti(3) and Ti(4); they are asymmetric and unequal with average values of 1.541(5)Å for P-O and 1.987(5)Å for Ti-O contacts in **1** and respectively, 1.543(7) Å for P-O and 2.008(7) Å for Ti-O in **2**. All titanium atoms are octahedrally
30 coordinated and connected to the central $\mu_4-O(1)$ atom. This triangular Ti_3O fragment is always present as a building block in the investigated oxo-alkoxo-titanate structures and can be regarded as a model for the Ti_3O triangular site exposed on the {100} and {101} faces of the TiO_2 nanoparticles with anatase
35 structure resulting from the sol-gel synthesis.
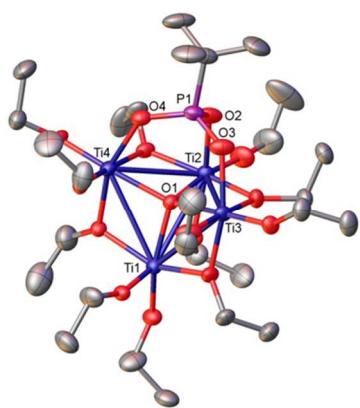
Fig. 1. Molecular structure of $Ti_4O(EtO)_{12}(^tBuPO_3)$, compound **1**. H-atoms and atom sites with minor disorder are omitted for clarity.

The structure of the derivative of aminoethyl phosphonic acid is
40 closely analogous, involving also a $Ti_4O(EtO)_{12}(RPO_3)$ unit (see Fig. 2). The presence of an amino group leads to a second coordination of $Ti_4O(EtO)_{12}(RPO_3)$ units with a $Ti_2(EtO)_8$

fragment and allows forming a Ti_{10}-complex. This structural behavior is not unexpected for the titanium alkoxides which
45 readily coordinate primary amines with formation of dimeric cores supported by hydrogen bonding. [32] It has to be mentioned that the involvement of the amino group into coordination in the alkoxide model cannot be considered as indication of its possible participation in direct coordination with Ti(IV) centers in the
50 neutral or weakly acidic aqueous medium, in which the adsorbent materials are applied, in the view that it is then coordination-inactive ammonium $-NH_3^+$ group that is present there instead of the donor $-NH_2$ one.
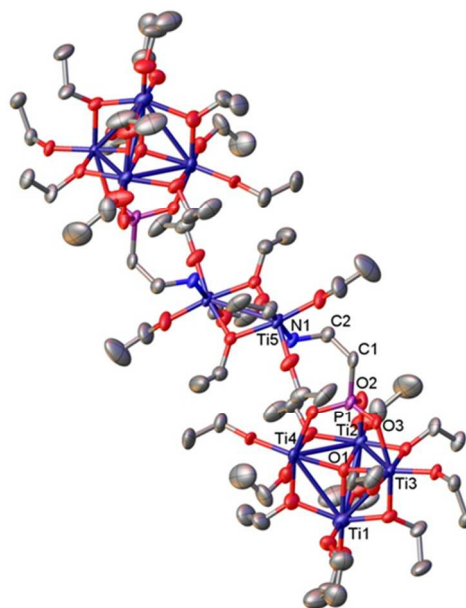
55 **Fig. 2.** Molecular structure of $Ti_{10}O_2(EtO)_{32}(AEP)_2$, compound **2** (b). H-atoms and atom sites with minor disorder are omitted for clarity.

An important question dealing with the grafting of ligands onto metal alkoxide surface is related to how densely the groups can be placed on the surface. An answer to this question can be
60 obtained via analysis of the known larger oxo-alkoxo-titanate structures bearing alkyl phosphonate ligands. In fact the size of the earlier investigated larger oligonuclear complexes bearing alkyl phosphonate ligands, for example, $Ti_{25}O_{26}(EtO)_{36}(PhenylPO_3)_6$ or $[Ti_{26}O_{26}(EtO)_{39}(PhenylPO_3)_6]^+$
65 ion, [25] is of ~2 nm for the largest dimension (the length of these non-spherical species). The distance between the phosphorus atoms grafted on the surface of these alkyl capped oxide nanoparticles, structurally related to anatase (see [32] for details), is practically constant and constitutes 8.67 Å ≈ 0.87 nm (see Fig. 3).
70 This permits to estimate the maximal theoretically possible coverage of the surface of titania nanoparticles giving minimal surface required per ligand unit to be $(0.87/2)^2 = 0.19$ nm^2. This value is slightly lower than the experimental value of 0.21 nm^2 per phosphonate ligand for the monolayer coverage of {100}
75 anatase face obtained experimentally (see [8] and refs therein) and permits to calculate maximum loading for the nanoparticle surface to be $(1m^2/0.19 \cdot 10^{-18}m^2)/6.022 \cdot 10^{23}mol^{-1} = 8.77 \cdot 10^{-6}$ mol/m^2 = 0.00877 mmol/m^2. For the active surface area ca. 100

m^2/g for aggregated nanoparticles, the maximal loading would be 0.877 mmol/g.
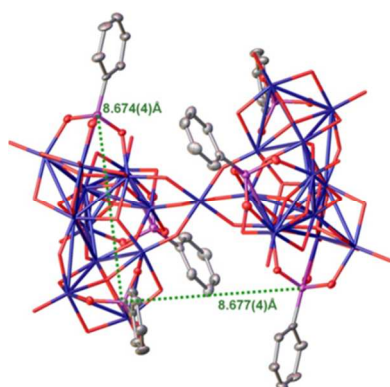
Fig. 3. Schematic presentation of $Ti_{25}O_{26}(EtO)_{36}(PhenylPO_3)_6$ according to [29] with indicated independent distances between phosphonate ligands; all other contacts are related by symmetry. H-atoms and ethyl groups on the surface of the Ti_{25}-cluster are omitted for clarity.

The observed loading on the surface of nano adsorbent (please, see below) is in the order of magnitude of one fourth of this value. This can be explained by the fact that the estimated density is related to fully open surface. In a mesoporous matrix with the pores having average size 4 nm and bottleneck connections as is the case with the applied TiO_2 material, [13] the ligand sizes of AEPA and IMPA ligands, taking into account the van-der-Waals radii, constituting 0.7 and 1.6 nm respectively, would thus be shielding approximately 75 % of the available surface, which correlates well with the data obtained in this work.

Synthesis and characterization of hybrid adsorbents

The active functions were introduced into forming hybrid adsorbent by grafting of a set of selected amino phosphonic acids, by direct adsorption of two chosen ligands – AEPA and IMPA. The ceramic yields for the adsorbents were for both ligands ~ 70%, and the inorganic-organic hybrid materials were separated by straightforward sedimentation overnight. The deviation from a quantitative yield was ascribed to a partial stabilization in solution of small and non-precipitating nanoparticle aggregates, splitting from the body of nanorods on mechanical treatment (stirring in 72 h), by the adsorbed amino phosphonic ligands. The adsorption of amino phosphonate ligands has already been reported to stabilize dispersions of small non-aggregated metal oxide nanoparticles. [8] The effect was more pronounced for AEPA than for IMPA, as it has been observed previously for other oxide systems. [8]

The powder XRD of the obtained hybrid material distinctly showed that the crystal structure of the nanoparticles (TiO_2/anatase) was conserved (see the diffractograms in Figure 4a). Moreover, even the EXAFS spectra (Figure 4b), which are highly sensitive to the local ordering in the structure, were practically the same as for bulk anatase TiO_2 [13] and the inorganic-hybrid sorbent TiO_2-AEPA. General features of the porous structures were determined by studying the adsorption and desorption of N_2 at a temperature of 77 K. The isotherms displayed in Fig. 4c show belongs to the type IV class when using the IUPAC's classification and the mesoporosity is preserved on surface grafting as manifested by similar type IV adsorption isotherms with characteristic hysteresis loop in the region of 0.5-0.8 P/P_s. The hysteresis loop closed at the same pressure for all the sorbents. Pore size distribution is displayed in Fig. 4d.
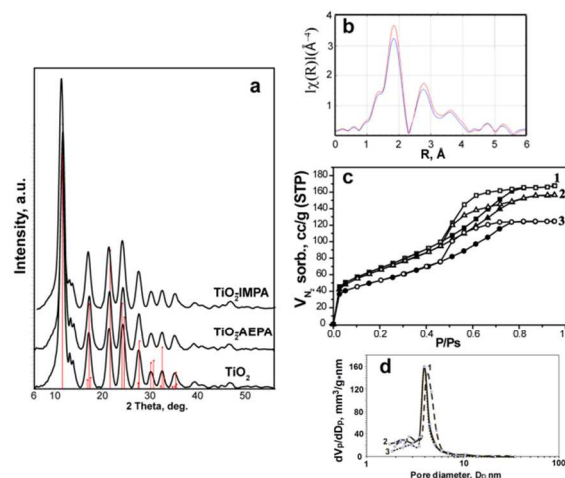
Fig. 4. Texture of initial and modified samples: (a) powder XRD of the samples (anatase – red lines); (b) The Fourier transformed and phase-corrected Ti EXAFS spectra for the starting nanorods (blue line) and the sample obtained by their modification by 2-aminoethyl phosphonic acid, AEPA (red line); (c) N_2 adsorption (●) – desorption (○) isotherms of samples TiO_2 (1), TiO_2-AEPA (2) and TiO_2-IMPA (3) and (d) Pore size distribution curves of samples TiO_2 (1), TiO_2-AEPA (2) and TiO_2-IMPA (3).

The closure at a relative pressure of 0.45 most probably correspond to the cavitation of N_2 [33] and the pores are probably ink-bottle shaped, which is in agreement with the expected structure built up of partially coalesced uniform-size nanoparticles. The active surface area were somewhat decreased for the modified TiO_2, especially for the TiO_2-IMPA sample.
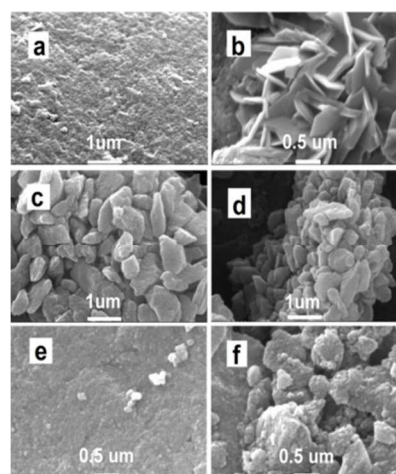
Fig. 5. SEM images of initial and modified samples: pure TiO_2 (a, b), TiO_2-AEPA (c, d), and TiO_2-IMPA (e, f).

The SEM images of the modified TiO_2 (see Figure 5) testify that no significant changes occur in the morphology of the samples as a result of surface grafting of AEPA and IMPA. The size of the primary nanoparticle aggregates were estimated to 60-70 nm for the non-modified TiO_2, and for the TiO_2-IMPA to 80-90 nm.

The content of AEPA and IMPA groups grafted on the TiO_2 surface is an important characteristic of the obtained materials. These amounts were determined from elementary microanalysis of phosphorus. Consistency checks for these amounts were performed by TGA, EDX analysis, and in case of the TiO_2-IMPA sample also from the data on potentiometric titration (the estimated standard deviations for each technique are provided in the Experimental Section).
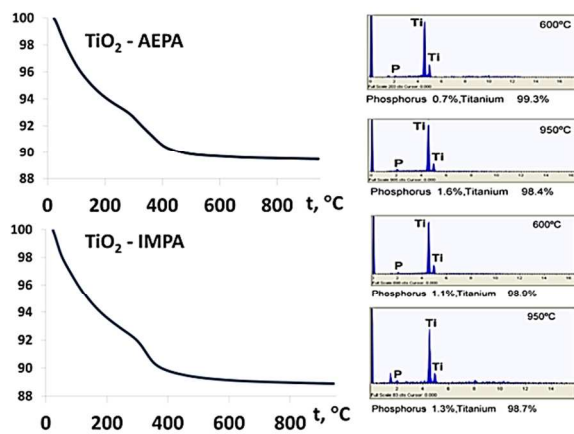
Fig. 6. Thermograms and EDS analysis for the TiO_2-phosphonate modified samples.

The results of these measurements are summarized in **Tab. 2**. It has to be noted that the results of TGA characterized by a small standard deviation have to be evaluated with caution as the thermal transformations at 650°C and even at 950°C are not resulting in complete removal of phosphorus. According to EDX, this outcome can be explained by a formation of poorly volatile phosphates (Fig. 6).

In total, taking into consideration the results from different techniques and their potential drawbacks and standard deviations, the content of grafted ligands could be estimated for the TiO_2-AEPA sample at 0.21 mmol/g and for the TiO_2-IMPA sample at 0.17 mmol/g. This correlates reasonably well with the monolayer coverage model earlier evaluated experimentally for dispersions of single nanoparticles subjected to grafting with phosphonic acids [8] and derived from the evaluation of the single crystal X-ray studies of the related molecular model compounds (please, see Figures 1-3 and the discussion above).

An indirect insight into surface coordination of the amino phosphonic acids onto TiO_2 is provided by their FTIR spectra (Figure 8). As reported in literature, [34] AEPA can form molecular zwitter-ionic structure in the spectrum of which the vibrational bands relating as to the bending NH_3^+ modes of the initial acid are located at 1482 cm^{-1} [$\delta_s NH_3$] and 1643 cm^{-1} [$\delta_{as}NH_3$]. During modification of the surface of titanium dioxide by AEPA the phosphonate groups are involved into complex formation and possibly deprotonation, leading for the TiO_2-AEPA sample to the

shift of the $\delta_s NH_3$ adsorption band to 1510 cm^{-1} (Figure 7).
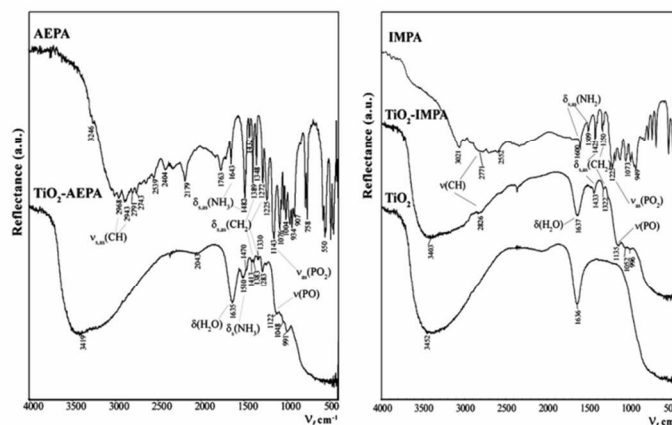
Fig. 7. DRIFT spectra for the initial acids and samples bearing grafted ligands.

Intensive absorption band at 1143 cm^{-1} for AEPA, which can be assigned to $\nu_{as}(PO_2)$ is for the TiO_2-AEPA sample shifted to 1122 cm^{-1}. There are similar effects for TiO_2-IMPA where the $\nu(PO)$ at 1225 cm^{-1} for pure IMPA is shifted to 1135 cm^{-1} for TiO_2-IMPA (Figure 8). The spectra of both samples containing grafted ligands (Figure 5) display a broad line at 500-800 cm^{-1} characteristic of the initial TiO_2 sample, $\nu(Ti-O)$, and also weak bands in the 1150-1500 cm-1 region associated with the bending vibrations of the methylene groups in the ligand structures. Medium intensity broad band at ~1635 cm^{-1}, present apparently due to $\delta(H_2O)$ vibrations, is masking supposedly the relatively weak $\delta_{as}NH_3$ bands. The FTIR spectra demonstrate thus that the ligands are definitely located on the surface after grafting and that at least AEPA is present there in zwitter-ionic form, indicating possibility that this acid can be connected to the TiO_2 surface with release of only one proton.

Additional insight into both grafting of the amino phosphonic acids and their interaction with Ln^{3+} cations on adsorption from solutions were obtained by solid state ^{31}P NMR spectroscopy. The ^{31}P NMR spectra of the TiO_2-IMPA samples all displayed a single peak at a chemical shift of 7.3 ppm. (Fig. FS2). Hence, it remained unaffected by adsorption of REE cations, which indicated that the latter are interacting with the ligand predominantly electrostatically. This ^{31}P NMR shift was similar to one of the two narrow lines observed by Bauer et al. for crystalline open-framework materials. [35] The ^{31}P NMR lines for the TiO_2-IMPA samples were broad as expected from the surface amorphous nature. The full width at half maximum was 9.3, 10, and 10.6 ppm for the TiO_2-IMPA, TiO_2-IMPA-La^{3+}, and TiO_2-IMPA-Y^{3+}. The ^{31}P NMR spectra of TiO_2-AEPA contain a dominant peak at ~20 ppm (18.8-20.8 ppm for the TiO_2-AEPA, TiO_2-AEPA-La^{3+}, and TiO_2-AEPA-Y^{3+} samples) and also a minor band at a chemical shift of ~ -2 ppm. The chemical shift of pure 2-aminoethanephosphonic acid is 19.1 and 18.9 ppm in solid and liquid state respectively. [36] The minor band at a low chemical shift was more prominent for the TiO_2-AEPA -Y^{3+} than for the TiO_2- AEPA-La^{3+} sample, the later had in turn a larger relative intensity of this band than did the TiO_2-AEPA.

Journal Name

ARTICLE TYPE

Table 2. Content of functional groups and structural-adsorption characteristics of obtained samples

Sample	Element analysis data, mass.% P	C_{acid}, mmol g^{-1} from P elem. anal.	Δm, % exc. water	C_{acid}, mmol g^{-1} from TGA	EDX data, mass. % P	C_{acid}, mmol g^{-1} from EDX anal.	C_{acid}, mmol g^{-1} from titration	$S_{sp.}$, m^2 g^{-1}	$V_{s.}$, cm^3/g	d, nm	C_{acid}, μmol/m^2 (unit/nm^2)
TiO$_2$	-	-	-	-	-	-	-	247	0.26	4.0^a/4.2^b	-
TiO$_2$-AEPA	0.65	0.21	3.96	0.32	0.4	0.13	Not determ.	239	0.24	3.9^a/4.0^b	0.8 (0.5)
TiO$_2$-IMPA	1.06	0.17	3.83	0.19	0.9	0.15	0.15	188	0.19	3.9^a/4.0^b	1.8 (1.1)

^{a}calculated using BJH method [31]
^{b}calculated using d=4V_s/S_{sp}

The reason for appearance of this band might be formation of an AEPA dimer species containing a P-O-P bond. The formation of the latter can potentially be catalyzed by rare earth cations. Building of such dimer species on interaction with sorbents has been observed for AEPA earlier. [37, 38] The observed ^{31}P NMR peaks are clearly shifted up-field compared to the signal in the fully covalently bound compound **1** (32.0 ppm). This is in excellent correlation with the generally observed trend of strong correlation of the downfield shift with the relative positive charge associated with the magnetized atom: the higher relative positive charge, the stronger positive shift in the NMR signal is observed. In the present case the highest shift 32.0 ppm is observed for compound **1** Ti$_4$O(EtO)$_{12}$(^{t}BuPO$_3$) (please, see below) with mostly covalent Ti-O-P bonds, followed by the free acids in the solid state (about 20 ppm) and then by more negatively charged ligand adsorbed on the surface, less than 10 ppm.

As indicated by the studies of the structures of molecular model compounds, the grafting occurs in all cases supposedly in a vertical tripod manner, but these tripods can be supposedly of different degrees of protonation. This result correlates reasonably well with the obtained NMR data in this work and those available in literature. [39] Reported in literature observation of multiple signals for the phosphonic acids bound to the oxide surfaces under more extreme conditions (higher temperatures and the removal of water under vacuum) indicates most probably simultaneous presence of several coordinated or even condensed forms. The crystallographically studied molecular models reveal often this type of inner-sphere chelated complexes. [31] The release of only one proton in the present case on adsorption of an acid might indicate grafting supported by additional hydrogen bonding as hypothesized in. [8]

Sorption kinetics of Dy^{3+} cations from aqueous solutions were investigated for both TiO$_2$-AEPA and TiO$_2$-IMPA (see Fig. 8). The dynamic equilibrium in REE adsorption was achieved for both TiO$_2$-AEPA and TiO$_2$-IMPA within 72 h. Such considerable delay in reaching the equilibrium is usually a feature of mass transport limitations within the materials. These limitations appear logical due to the ink-bottle shaped pores that were indicated in the N$_2$ desorption characteristics in these adsorbents. The Dy^{3+} adsorption by TiO$_2$-IMPA was faster than on TiO$_2$-AEPA, and was completed to 95% within 24 h.
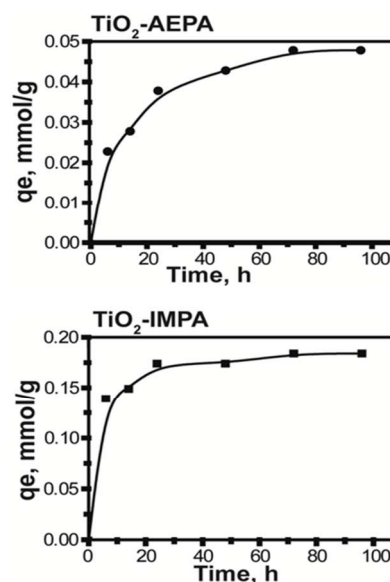
Fig. 8. Kinetics of Dy^{3+} ions sorption by samples TiO$_2$-IMPA and TiO$_2$-AEPA.

The sorption isotherms obtained for Y^{3+}, La^{3+}, Nd^{3+} and Dy^{3+} cations (see Fig. 9 and **Tab. TS2**, **TS3**) belong to the Langmuir type indicating similar sorption mechanisms in all cases. All isotherms had slight kinks in the equilibrium concentration region of 0.05-0.2 mmol/l. These kinks could speculatively indicate potential conformational changes for the ligands in the surface layer on TiO_2 or testify the presence of two different adsorption sites. It may be supposed that for smaller AEPA molecules a more pronounced difference between the adsorption sites on the surface of the material and inside the pores can be observed. As indicated in **TS2** and **TS3** the sorption of Ln^{3+} cations caused a pH decrease in solution, which meant that this process was associated with deprotonation of the ligands located on the surface of TiO_2. The sorption on TiO_2-AEPA (**Tab. TS2**) led to a release of one proton per each adsorbed metal ion, while for TiO_2-IMPA (**Tab. 2**) a release of ~3 protons was observed (i.e. grafting on the surface of TiO_2 was thus in both cases associated with a release of only one proton as was deduced from the data on potentiometric titration). Note that while the Ln^{3+}:L ratio lies for TiO_2-AEPA in a relatively broad range 1:2.4 (Dy) – 1:4.5 (Y), for the TiO_2-IMPA sample it is close to 1:1 [1:0.7(Dy) – 1:0.94(Y)] (see **Table TS2**).
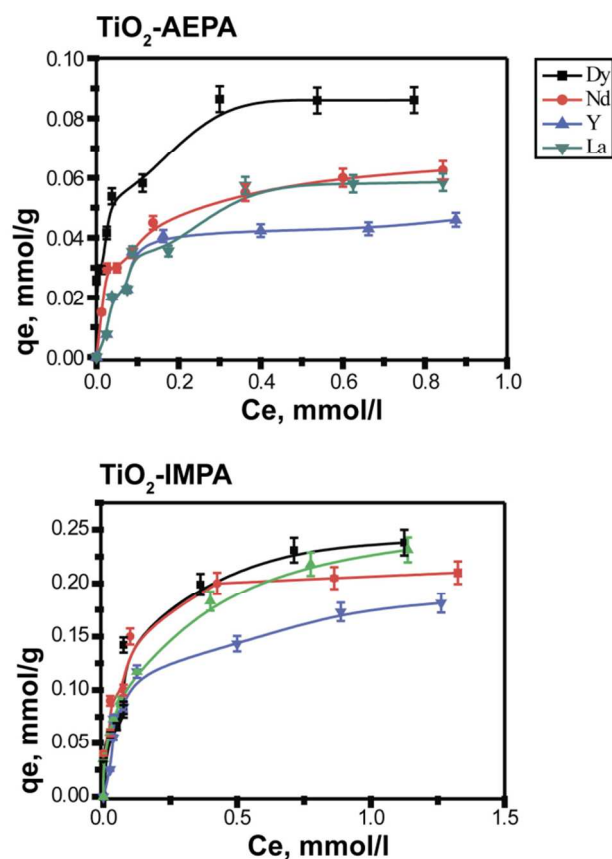
Fig. 9. Sorption isotherms of Nd^{3+}, Dy^{3+}, Y^{3+} and Ln^{3+} on TiO_2, functionalized with aminophosphonic acids.

This implies that in the latter case similar 1:1 complexes were formed, which was in agreement with the released number of protons per each formed complex (on condition that the grafting

itself occurs with deprotonation of only one P-OH group). In the view that the sorption occurred at relatively low pH (about 3) the amino groups of the ligands remained protonated, and were not involved in complexation. The composition of the complexes had thus to be driven by the charge compensation principle, leading to L : M^{3+} ratios 1 : 1 for IMPA (triply-charged anion $(O^-)_2P(=O)(O-Ti)-CH_2NH_2^+-CH_2P(=O)(O^-)_2$) and about 3:1 for AEPA (single-charged anion $H_3N^+-CH_2CH_2P(=O)(O-Ti)O^-$). Potential density of OH-groups on the flat anatase surface permits to consider the formation of an LnL_3 complex with AEPA. [40] This, however, can be questioned for the AEPA in the view that the pH measurements indicate evolution of only one proton on adsorption of Ln^{3+}. An alternative explanation can be that the smaller AEPA ligands are not always available for interactions with the rare earth cations and only formation of complexes with 1:1 composition takes place. Such hinders for complexation may arise because of the surface roughness of applied matrix on the nano level. For the TiO_2-IMPA sample the quantity of adsorbed cations was slightly, but noticeably exceeding that to be expected from the exact Ln^{3+}:L = 1:1 ratio (see **Tab. TS2**). This might indicate some additional sorption mechanism realized to minor extent, possibly formation of electrostatically bound outer sphere complexes etc.

The results of EDX analysis of the contents of phosphorus and the adsorbed metals for the samples corresponding to final points in the sorption isotherms (**Fig. 9**) are summarized in **Table TS1** together with the L:Ln^{3+} ratios derived from them. It has to be mentioned that they do not always appear to be in agreement with the data obtained in the sorption experiments. This is especially apparent for the Y^{3+} cation and the TiO_2-AEPA sorbent (see **Tab TS2** and **TS3**). In case of this adsorbent good agreement for the L:Ln^{3+} ratios is observed only for Nd^{3+} (3.3, see Table 3), while for La^{3+} and Dy^{3+} cations they are relatively close but display an inverted trend (please, compare **Table TS3** and **Table TS1**). For the TiO_2-IMPA samples, the agreement between the L:Ln^{3+} ratios calculated from EDX analysis for the La^{3+} and Nd^{3+} ions is considerably higher (see **Tab. TS1**), being close to 2:1, while for the Dy^{3+} ion it is a bit less, 1.5:1 (see **Tab. TS1**). It has to be noted that the EDX data in this case (**Tab. TS1**) are apparently less reliable than the data derived from titration experiments (**Tabs. TS2** and **TS3**): the morphology of the adsorbents is quite complex with pronounced roughness at the nano level, which can lead to scattering of the secondary X-ray radiation used in the analysis and affect the determined relative content of light and heavy elements (P:Ln ratio used for estimation of the complex composition in EDX). The produced adsorbents reveal some visible difference in capacity towards different REE with distinctly better uptake of Dy^{3+}, compared to bigger (La^{3+} and Nd^{3+}) and much smaller (Y^{3+}) cations. This difference can be caused by matching the size of the cation with the negatively charged coordinated environment provided by the immobilized ligands on the surface. In case of iminodiacetic acid as active adsorption function such effects have recently been revealed and explained with the help of available molecular model structures. [14e]

The obtained adsorbents show thus quite modest values of static sorption capacity (SSC) and distribution coefficient Q (see **Tab. TS1**) compared with the best silica-based mesoporous

nanoadsorbents constituting the state-of-the-art in the field. [14,41] It is important to note that also the electrostatic/ion exchange mechanism of adsorption revealed in this case is going to provide less selective binding compared to chelating or specifically coordinating ligands.[14] Phosphonate adsorption functions are active even in the binding of actinides, potentially limiting application of the developed adsorbents to sources not contaminated heavily with the latter. However, our results are impressively better than those from analogous experiments with hybrid organic-inorganic adsorbents based on ZrTi-0.33 mesoporous adsorbent functionalized with, in particular, amino tris(methylphosphonic) acid: the TiO_2-AEPA shows about 10 times and TiO_2-IMPA up to 50 times higher adsorption capacity. [23] Much lower price of mesoporous titania prepared by the utilized approach makes the produced material potentially interesting for remediation applications. The better efficiency in ligand involvement in adsorption revealed by the TiO_2-IMPA material provides it with 3-4 times higher capacity compared with TiO_2-AEPA. The kinetics of the adsorption process in the present case was extremely slow due, supposedly to strong aggregation of the applied microparticles. It may, hopefully be improved via sonication of the suspensions, which, however at the same time become more difficult to separate by sedimentation. A possible option for application of the produced materials can be in water remediation, where longer contact with solutions in sedimentation baths is not a hinder.

We have investigated even the perspective of application of the produced adsorbents for recuperation of REE by desorption and also for repeated application. As indicated by the data in the **Table 3**, desorption of Dy^{3+}-cations by 1 M hydrochloric acid is practically complete (ca 95%). The uptake of the Dy^{3+} ions on repeated sorption with the thus cleaned adsorbent turns, however, to be noticeably less efficient – 68% on TiO_2-IMPA and only 27% for TiO_2-AEPA compared with the original material (see **Tab. 5**). It cannot be excluded that especially in case of AEPA even a partial loss of the grafted ligand takes place.

Table 3. Sorption-desorption investigation of Dy^{3+}.

Sample	1st sorption, mmol/g	Desorption, mmol/g	Desorption, %	2nd sorption, mmol/g	Resorption, %
TiO_2-IMPA	0.184	0.175	95	0.119	68
TiO_2-AEPA	0.048	0.045	94	0.013	27

Partial loss of the ligand on desorption can supposedly be avoided using other desorbing reagents than hydrochloric acid. In particular, the application of ammonium sulfate for desorption of REE from solid adsorbents has been proposed.[42] In fact, the stability of phosphonate adsorbents in different media has recently attracted much attention. In particular, application of porous and poorly soluble metal phosphonates with enhanced stability in acidic medium has been reported.[43]

Conclusions

The grafting of phosphonate ligands onto a metal oxide surface occurs apparently in the tripod vertical fashion, the difference between the observed NMR shifts resulting most probably from different protonation. By comparing the data from several experimental methods (FTIR, TGA and EDS analysis) it appeared as the ligands are bound to the TiO_2 surface through loss of one proton per ligand.

The investigation of the molecular model compounds permits to set the limit of the area for a phosphonate function for monolayer coverage at 0.19 nm^2 for nanoparticle substrate, which is slightly lower than the value observed for monolayer coverage on {100} anatase surface (0.21 nm^2).[8] The composition of the produced hybrid nano materials was in agreement with this finding, taking into account the shape and size of pores in the applied mesoporous matrix.

A simple and efficient methodology for preparation of hybrid adsorbents based through grafting of amino phosphonate ligands on the surface of mesoporous titanium dioxide was developed. The ligand loading varies for different ligands in the range 0.17-0.21 mmol/g. The pore volume and active surface area undergo minor decrease as a result of this transformation. The structure and morphology of the initial mesoporous nanomaterial were according to the data of powder XRD and EXAFS studies preserved intact.

The adsorption of REE, Y^{3+}, La^{3+}, Nd^{3+} and Dy^{3+}, cations from weakly acidic solutions was associated with a considerable decrease in the pH, which indicating an ion exchange mechanism for this process. The complexes contained statistically about 3 phosphonate groups per metal atom corresponding to ML_3 composition for TiO_2-AEPA and ML composition for TiO_2-IMPA adsorbent. This picture is in agreement with the idea about mostly electrostatic nature of interaction in the inner-sphere complexes and that their composition is driven by the charge compensation principle. An alternative explanation for AEPA can be formation of a complex with 1:1 composition with simultaneous shielding of a large part of the smaller ligands because of the surface roughness at the nanometer scale level. The adsorbed metal ions can be released with 95% efficiency by washing the loaded adsorbent with 1 M hydrochloric acid, but the recuperated adsorbent loses at least part of its activity (about 30% for TiO_2-IMPA and 70% for TiO_2-AEPA). Produced materials may be of interest in extraction of REE and in water remediation applications.

Acknowledgments

Notes and references

a Department of Chemistry and Biotechnology, Biocenter, Swedish University of Agricultural Sciences, Box 7015, 750 07 Uppsala, Sweden, E-mail: Gulaim.Seisenbaeva@slu.se; Vadim.Kessler@slu.se

b Chuiko Institute of Surface Chemistry, National Academy of Sciences of Ukraine, 17, General Naumov Street, Kyiv 03164 Ukraine;; E-mail: in.melnyk@gmail.com; yurii.zub@gmail.com

c Berzelii Centre EXSELENT, Department of Materials and Environmental Chemistry, Arrhenius Laboratory, Stockholm University, 106 91 Stockholm, Sweden; E-mail: Niklas.hedin@mmk.su.se

d Department of Chemistry, University at Buffalo, SUNY, Buffalo, NY 14260-3000, USA.; E-mail: elzbieta@buffalo.edu

† Electronic Supplementary Information (ESI) available: tables with the summary of the data of TGA, EDS, potentiometric and elementary microanalysis and the ^{31}P NMR spectra.. See DOI: 10.1039/b000000x/

‡ Footnotes should appear here. These might include comments relevant to but not central to the matter under discussion, limited experimental and spectral data, and crystallographic data.

1 X.L. Qu, J. Brame, Q.L. Li, P.J.J. Alvarez, *Acc. Chem. Res.*, 2013, **46**, 834.

2 Y. Chen, Y.Y. Yi, J.D. Brennan, M.A. Brook, *Chem. Mater.,* 2006, **18**, 5326.

3 B.A. Gregg, *Chem. Rev.*, 2004, **248**, 1215.

4 T. Preocanin, N. Kallay, *Croat. Chem. Acta*, 2006, **79**, 95.

5 M. Bonato, K.V. Ragnarsdottir, G.C. Allen, *Water Air Soil Pollut.,* 2012, **223**, 3845.

6 a) X.H. Guan, J.S. Du, X.G. Meng, Y.K. Sun, B. Sun, Q.H. Hu, *J. Hazard. Mater.,* 2012, **215-216**, 1; b) T.S. Anirudhan, L. Divya, J. Parvathy, *J. Chem. Technol. Biotechnol.,* 2013, **88**, 878; c) M.I. Danish, I.A. Qazi, A. Zeb, A. Habib, M.A. Awan, Z. Khan, *J. Nanomaterials,* 2013, Article ID 873694; d) Y.C. Tang, C.N. Wu, X.H. Huang, H.P. Zhang, H.Q. Yu, X. Li, Y. Peng, *Desalin. Water Treatm.*, 2012, **49**, 359.

7 Q.L. Zhang, L.C. Du, Y.X. Weng, L. Wang, H.Y. Chen, J.Q. Li, *J. Phys. Chem. B*, 2004, **108**, 15077.

8 R. Pazik, R. Andersson, L. Kepinski, V.G. Kessler, J.M. Nedelec, G.A. Seisenbaeva, *J. Phys. Chem. C,* 2011, **115**, 9850.

9 a) S. Monti, T.R. Walsh, *J. Phys. Chem. C,* 2011, **115**, 24238; b) H.J. Cleaves, C.M. Jonsson, C.L. Jonsson, D.A. Sverjensky, R.M. Hazen, *Astrobiol.*, 2010, **10**, 311.

10 E. Topoglidis, A.E.G. Cass, G. Gilardi, S. Sadeghi, N. Beaumont, J.R. Durrant, *Anal. Chem.*, 1998, **70**, 5111.

11 a) F.F. Rossetti, M. Textor, I. Reviakine, *Langmuir*, 2006, **22**, 3467; b) Y.V. Kolen'ko, K.A. Kovnir, A.I. Gavrilov, A.V. Garshev, J. Frantti, O.I. Lebedev, B.R. Churagulov, G. Van Tendeloo, M. Yoshimura, *J. Phys. Chem. B*, 2006, **110**, 4030.

12 J. Choi, A. Ide, Y.B. Truong, I.L. Kyratzis, R.A. Caruso, *J. Mater. Chem. A,* 2013, **1**, 5847.

13 G.A. Seisenbaeva, G. Daniel, J.M. Nedelec, Y.K. Gun'ko, V.G. Kessler, *J. Mater. Chem.*, 2012, **22**, 20374.

14 a) J. Florek, F. Chalifour, F. Bilodeau, D. Larivière, F. Kleitz, *Adv. Funct. Mater.,* 2014, **24**, 2668; b) S.K. Das, M.K. Bhunia, A. Bhaumik, *Micropor. Mesopor. Mater.*, 2010, **128**, 34; c) I. Sierra , D. Pérez-Quintanilla , *Chem. Soc. Rev.,* 2013 , **42**, 3792; d) S. Demirel Topel, E. Polido Legaria, C. Tiseanu, J. Rocha, J.M. Nedelec, V.G. Kessler, G.A. Seisenbaeva, *J. Nanopart. Res.*, 2014, **16**, 2783; e) E. Polido Legaria, S. Demirel Topel, V.G. Kessler, G.A. Seisenbaeva, *Dalton Trans.*, 2015, **44**, 1273.

15 a) T. Arita, K. Moriya, T. Yoshimura, K. Minami, T. Naka, T. Adschiri, *Ind. Eng. Chem. Res.,* 2010, **49**, 9815.; b) B. Faure, G. Salazar-Alvarez, A. Ahniyaz, I. Villaluenga, G. Berriozabal, Y.R De Miguel, L. Bergström, *Sci. Technol. Adv. Mater.,* 2013, **14,** 023001.

16 a) F.J. Song, Y.X. Zhao, H.L. Ding, Y. Cao, J. Ding, Y.F. Bu, Q. Zhong, *Environ. Tech.,* 2013, **34**, 1405; b) F.J. Song, Y.X. Zhao, H.L. Ding, Y. Cao, J. Ding, Y.F. Bu, Q. Zhong, *Appl. Surf. Sci.,* 2013, **268**, 124.

17 a) N. Sridewi, Y.F. Lee, K. Sudesh, *Int. J. Photoenergy*, 2011, **2011**, 597854; b) J.J. Li, J.T. Feng, W. Yan, *J. Appl. Polymer Sci.*, 2013, 3231.

18 S. Abbasizadeh, A.R. Keshtkar, M.A. Mousavian, *Chem. Eng. J.*, 2013, **220**, 161.

19 X.Q. Cao, *J. Mater. Sci. Tech.,* 2007, **23**, 15.

20 A.J. Hurd, R.L. Kelley, R.G. Eggert, M.H. Lee, *MRS Bull.*, 2012, **37**, 405.

21 S. Schneider, C. Walther, S. Bister, V. Schauer, M. Christl, H.A. Synal, K. Shozugawa, G. Steinhauser, *Sci. Rep.*, 2013, **3**, 2988.

22 I.V. Melnyk, V.P. Goncharyk, N.V. Stolyarchuk, L.I. Kozhara, A.S. Lunochkina, B. Alonso, Y.L. Zub, *J. Porous. Mater.*, 2012, **19**, 579.

23 C.S. Griffith, M. De Los Reyes, N. Scales, J.V. Hanna, V. Luca, *ACS Appl. Mater. Interfaces*, 2010, **2**, 3436.

24 G.A.; Seisenbaeva, V.G. Kessler, *Nanoscale*, 2014, **6**, 6229.

25 Y. Chen, E. Trzop, J.D. Sokolow, P. Coppens, *Chem. Eur. J.,* 2013, **19**, 16651.

26 S. Brunauer, P. H. Emmett, E. Teller, *J. Am. Chem. Soc.,* 1938, **60**, 309.

27 E.P. Barrett, L.G. Joyner, P.P. Halenda, *J. Am. Chem. Soc.,* 1951, **73**, 373.

28 M. Newville, *J. Synchrotron Rad.*, 2001, **8**, 322.

29 G. Schwarzenbach, H.A. Flaschka, *Complexometric Titrations*. Methuen, London, 1967, 360.

30 G.M. Sheldrick, *Acta Cryst.*, 2008, **A64**, 112.

31 P. Coppens, Y. Chen, E. Trzop, *Chem. Rev.*, 2014, **114**, 9645.

32 U. Schubert, *Acc. Chem. Res.*, 2007, **40**, 730.

33 P.I. Ravikovitch, A.V. Neimark, *Langmuir,* 2002, **18**, 9830.

34 M.L. Roldán, A.E. Ledesma, A.B. Raschi, M.V. Castillo, E. Romano, S.A. Brandán, *J. Molecul. Struct.*, 2013, **1041**, 73.

35 S. Bauer, H. Müller, T. Bein, N. Stock, *Inorg. Chem.,* 2005, **44**, 9464.

36 R.K. Harris, L.H. Merwin, G. Hägele, *Magn. Reson. Chem.,* 1989, **27**, 470.

37 J.E. Cockburn, A.P. Williams, *J. Chromatogr. A,* 1982, **249**, 103.

38 N. Bibent, T. Charpentier, S. Devautour-Vinot, A. Mehdi, P. Gaveau, F. Henn, G. Silly, *Eur. J. Inorg. Chem.,* 2013, 2350.

39 G. Guerrero, P. H. Mutin, A. Vioux, *Chem. Mater.*, 2001, **13**, 4367.

40 C.B. Mendive, T. Bredow, A. Felthof, M.A. Blesa, D. Bahnemann, *Phys. Chem. Chem. Phys.*, 2009, **11**, 1794.

41 a) M.R. Awual, T. Kobayashi, Y. Miyazaki, R. Motokawa, H. Shiwaku, S. Suzuki, Y. Okamoto, T. Yaita, *J. Hazardous Mater.*, 2013, **252-253**, 313; b) M.R. Awual, T. Kobayashi, H. Shiwaku, Y. Miyazaki, R. Motokawa, S. Suzuki, Y. Okamoto, T. Yaita, *Chem. Eng. J.,* 2013, **225**, 558.

42 G.A. Moldoveanu, V.G. Papangelakis, *Hydrometallurgy*, 2013, **131-132**, 158.

43 A. Dutta, A.K. Patra, A. Bhaumik, *Micropor. Mesopor. Mater.*, 2012, **155**, 208.

GRABS SYNOPSIS

Organic-inorganic hybrid adsorbents with high capacity to adsorption of rare earth elements have been prepared through grafting of amino phosphonic acid ligands onto mesoporous TiO_2 under mild conditions. Their structure and maximal capacity was elucidated with the help of single crystal X-ray diffraction of molecular model compounds.

GRABS GRAPHIC